Scientia Iranica, Vol. 13, No. 3, pp 245–254

SCIENTIA IRANICA

Effect of Unsteady Friction Models and Friction-Loss Integration on Transient Pipe Flow

A. Vakil[1] and B. Firoozabadi*

When velocities in the piping systems change rapidly, spectacular accidents occur, due to transient-state pressures where the elastic properties of the pipe and liquid must be considered. This hydraulic transient is commonly known as water hammer. A conventional widely-used technique for analyzing this phenomenon is the Method Of Characteristic (MOC), in which, by introducing the characteristic lines, two ordinary differential equations, in lieu of the governing partial differential equations, are produced. In the undisturbed form of the equations, the energy dissipation is evaluated by the steady or quasi-steady approximation. But, there is experimental and theoretical evidence which shows that the velocity profiles in unsteady-flow conditions have greater gradients and, thus, greater shear stresses, than corresponding values in steady-flow. Moreover, the numerical integration of the friction-loss is based on the values at the previous time step. This paper employs the External Energy Dissipator, Karney's method, to apply the boundary conditions in a network. To investigate the effect of the unsteady friction formula, the cross characteristic mesh, based on the Vitkovsky formulation, is completely derived and incorporated in the network. At last, the effect of the weighting term in the integration of the friction-loss term is examined. The paper shows that if the maximum head rise were to be practically considered, it would not need the unsteady friction term to be taken into account. Moreover, the weighting integration constant has the slightest effect on the text network.

INTRODUCTION

It has been shown, both theoretically and experimentally, that in unsteady pipe flows, the energy dissipation experienced by fluid is by far greater than that experienced by steady flows [1-4]. The steady or quasi-steady friction approximation underestimates the shear stress and fails to correctly predict the peculiar events occurring. Therefore, advanced 1D and 2D models have been developed [5,6]. The 2D models stem from wave motion and turbulent diffusion are robust to handle [7-9]. But, there are two main approaches in considering unsteadiness during transient-state conditions in 1D models. One is based on the past flow acceleration [1]; the other depends on the instantaneous values of acceleration [10]. Referring to these models, there is a significant deviation from uniform flow profiles and the shear stress is out of phase with the mean velocity. To express deviation from the steady-state conditions, Zielke related the wall shear stress in transient laminar pipe flow to the instantaneous mean velocity and to the weighted acceleration history [1]. Since Zielke's model is memory-consuming, other researchers have developed approximations to it [11-13]. Zielke's family of models is also known as frequency-dependent friction models. The Brunone model relates the unsteady shear stress to instantaneous local acceleration $\frac{\partial V}{\partial t}$ and instantaneous convective acceleration $\frac{\partial V}{\partial x}$, by means of the coefficient, k, which can be estimated from Vardy and Brown's shear decay coefficient C^* [14] or by trial and error. This model is valid for a wide range of Reynolds number, including laminar or turbulent flows. The original Brunone model has been shown to be erroneous in predicting the acceleration phase. Vitkovsky improved the Brunone model to be in agreement with any type of acceleration or deceleration phase [15]. To reduce the number of boundary conditions and facilitate the calculation of transient conditions, Karney developed an efficient method, known as the External Energy Dissipator (EED) [16].

This paper reviews the unsteady friction model,

1. *Department of Mechanical Engineering, Sharif University of Technology, Tehran, I.R. Iran.*

*. *Corresponding Author, Department of Mechanical Engineering, Sharif University of Technology, Tehran, I.R. Iran.*

based on the Brunone model, and incorporates this model into Karney's efficient model. Results are verified on the test network presented in [16].

In the following section, the governing equation will be reviewed. Then, method of characteristics, the unsteady friction models and the external energy dissipator (EED) will be presented. After that, the cross characteristic method will be derived and a comparison will be made between the quasi-steady and Brunone models for two different cases on the text network, as described.

GOVERNING EQUATIONS

The momentum and continuity equations, describing the unsteady pipe flow, are a set of 1D qausi-linear hyperbolic partial differential equations [17,18]. These equations can be written in the following form:

$$L_1 = gH_x + V_t + VV_x + gh_f = 0, \tag{1}$$

$$L_2 = gH_t + a^2V_x = 0, \tag{2}$$

in which:

x	distance along pipe,
t	time,
$H = H(x,t)$	piezometric head,
$V = V(x,t)$	fluid velocity,
a	wave speed,
g	gravitational acceleration.

The head loss, due to fluid friction per unit length, ϕ_L, can be derived from the dissipation function [6]:

$$\phi_L = \frac{\partial u}{\partial r}\left(\mu\frac{\partial u}{\partial r} \quad \rho\overline{u'v'}\right), \tag{3}$$

where u is the axial velocity, r is the radial coordinate, $\frac{\partial u}{\partial r}$ is the velocity gradient in the radial direction and $\rho\overline{u'v'}$ is the Reynolds stresses for turbulent flow. By applying the Hagen-Poiseulle velocity profile, the energy loss per unit weight of liquid in a unit length of pipe for steady-state flow conditions is given by the following:

$$h_f = \frac{fV^2}{2gD}, \tag{4}$$

which is the same as the Darcy-Weisbach equation.

To consider the opposite direction of the flow, Equation 4 is written as below:

$$h_f = \frac{fV|V|}{2gD}. \tag{5}$$

The behavior of the friction factor can be defined by the implicit Colebrook-white equation [19].

METHOD OF CHARACTERISTICS

Equations 1 and 2 can be transformed into a set of ordinary differential equations, which are valid only on the appropriate characteristic lines [17,18]. The MOC combines the continuity and momentum equations with an unknown multiplier, λ.

$$L = L_1 + \lambda L_2. \tag{6}$$

If the convective term is small and the head loss can be approximated by Equation 5, the MOC can be defined in terms of discharge, Q, and head, H, as follows:

C^+ :

$$\frac{gA}{a}\frac{dH}{dt} + \frac{dQ}{dt} + f\frac{Q|Q|}{2DA} = 0, \tag{7}$$

$$\frac{dx}{dt} = a, \tag{8}$$

C :

$$\frac{gA}{a}\frac{dH}{dt} + \frac{dQ}{dt} + f\frac{Q|Q|}{2DA} = 0, \tag{9}$$

$$\frac{dx}{dt} = \quad a. \tag{10}$$

Equations 7 and 9 are now integrated along the C^+ and C , respectively (see Figure 1). To integrate the friction term, a linearization is used as follows [16]:

$$\int_{i\ \ 1,t\ \ \Delta t}^{i,t} Q|Q|\,dx = \Big[Q_{i\ \ 1,t\ \ \Delta t} + \varepsilon\left(Q_{i,t} \quad Q_{i\ \ 1,t\ \ \Delta t}\right)\Big]\left|Q_{i\ \ 1,t\ \ \Delta t}\right|\Delta x. \tag{11}$$

Two equations for the unknowns H and Q at (i,t) may

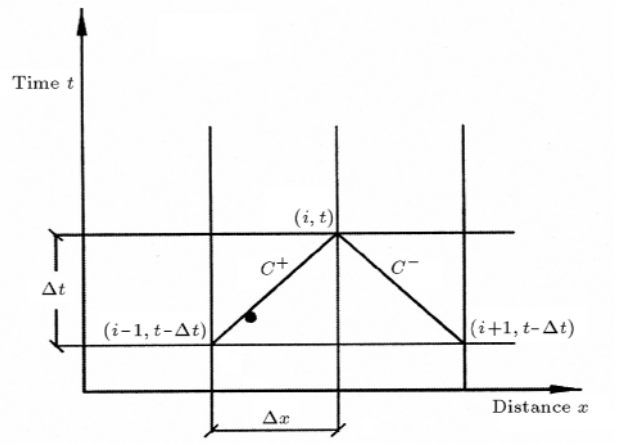

Figure 1. The x t grid showing characteristics for Equations 8 and 10.

be written as:

$$H_{i,t} = C_{c^+} \quad B_{c^+} Q_{i,t}, \tag{12}$$

and:

$$H_{i,t} = C_c \quad B_c \; Q_{i,t}, \tag{13}$$

where:

$$C_{c^+} = H_{i\ 1,t\ \Delta t} + Q_{i\ 1,t\ \Delta t}[B \quad R\,|Q_{i\ 1,t\ \Delta t}|\,(1 \quad \varepsilon)], \tag{14}$$

$$B_{c^+} = B + \varepsilon R\,|Q_{i\ \ 1,t\ \ \Delta t}|\,, \tag{15}$$

$$C_c = H_{i+1,t\ \ \Delta t} \; Q_{i+1,t\ \ \Delta t}\,[B \; R\,|Q_{i+1,t\ \ \Delta t}|\,(1 \quad \varepsilon)]\,, \tag{16}$$

$$B_c = B + \varepsilon R\,|Q_{i+1,t\ \ \Delta t}|\,, \tag{17}$$

where $B = \frac{a}{gA}$, $R = \frac{f\Delta x}{2gDA^2}$, A = cross-sectional area of the pipe and ε is the linearization constant.

The values of the constants C_{c^+}, B_{c^+}, B_c and C_c are known from the previous time step. Therefore, one can proceed in time by simultaneously solving Equations 12 and 13.

UNSTEADY FRICTION MODELS

Original and Modified Brunone Model

If the friction factor in Equation 5 is split into two components, quasi-steady f_q and unsteady component f_u, i.e., $f = f_q + f_u$, the Brunone model component can be defined by [10]:

$$f_u = \frac{kD}{V\,|V|}\left(\frac{\partial V}{\partial t} \quad a\frac{\partial V}{\partial x}\right). \tag{18}$$

The Vitkovsky's modified formulation, which takes into account the correct sign of the convective term, is as follows [10]:

$$f_u = \frac{kD}{V\,|V|}\left(\frac{\partial V}{\partial t} + a\ \mathrm{Sign}\,(V)\left|\frac{\partial V}{\partial x}\right|\right), \tag{19}$$

Sign(V) takes $+1$ for $V \geq 0$ and $\quad 1$ for $V < 0$.

The coefficient, k, can be found empirically or from Vardy's shear decay coefficient, C^*, as follows [14]:

$$k = \frac{\sqrt{C^*}}{2},$$

$$C^* = 0.00476 \quad \text{for laminar flow,} \tag{20}$$

$$C^* = \frac{7.41}{\mathrm{Re}^{\log_{10}\left(\frac{14.3}{\mathrm{Re}^{0.05}}\right)}} \quad \text{for turbulent flow.} \tag{21}$$

Zielke Model

By taking into account distortion of the traveling wave through frequency-dependent friction for an unsteady friction term in discrete form, Zielke derives the following equation [2]:

$$(f_u)_{i,k} = \frac{32\nu}{DV_{i,k}\,|V_{i,k}|}\sum_{j=1,3,\cdots}^{k\ \ 1}(V_{i,j+1\ \ 1} \quad V_{i,j\ \ 1})W((k \quad j)\Delta t)\,, \tag{22}$$

where i and k refer to the ith cross-section and kth time step, respectively. It should be noted that the weight function, W, for the past acceleration, is a function of the dimensionless time, τ;

$$W(\tau) = e^{\ 26.3744\tau} + e^{\ 70.8493\tau} + e^{\ 135.0198\tau} + e^{\ 218.9216\tau} + e^{\ 322.5544\tau}, \tag{23}$$

for $\tau \geq 0.02$,

$$W(\tau) = 0.282095\tau^{\ \frac{1}{2}} \quad 1.25000 + 1.057855\tau^{\frac{1}{2}} + 0.937500\tau + 0.396696\tau^{\frac{3}{2}} \quad 0.351563\tau^2, \tag{24}$$

for $\tau < 0.02$,

where $\tau = \frac{4\nu}{D^2}t$.

Since the method introduced by Zielke requires storage of all velocities computed at the previous time steps, the improved approximate method for simulating frequency-dependent friction in transient laminar flow has been devised [11-13].

EXTERNAL ENERGY DISSIPATOR (EED)

At boundary reaches, only one of the characteristic equations is available in the two variables, therefore, Equations 12 and 13 should be solved simultaneously with the conditions imposed by the boundary. The EED [16] reducing the number of boundary conditions should be defined to close the systems of equations. Based on the uniqueness of the head and continuity at the frictionless junction (where boundary section meet), Equations 12 and 13 lead to:

$$H_{i,t} = C_c \quad B_c Q_{\mathrm{ext}}, \tag{25}$$

in which:

$$B_c = \left(\sum_i \frac{1}{B_{c_i^+}} + \sum_i \frac{1}{B_{c_i}}\right)^{\ 1}, \tag{26}$$

and:

$$C_c = B_c\left(\sum_i \frac{C_{c_i^+}}{B_{c_i^+}} + \sum_i \frac{C_{c_i}}{B_{c_i}}\right)^{\ 1}. \tag{27}$$

Equation 25 represents a single relationship between junction head $H_{i,t}$ and external flow Q_{ext} in a frictionless junction. Generalized external dissipaters include tank, connector, valve/orifice and reaching pipe. The external flow can be expressed in terms of the head at the junction as follows:

$$Q_{\text{ext}} = s\tau E_s\sqrt{s\,(H_{i,t} \quad H_c^p)}, \tag{28}$$

where, H_p^c is the head at the node side of the connector, $s = \text{Sign}(Q_{\text{ext}}) = \pm 1$ and E_s and τ are valve/orifice parameters. Karney shows that Q_{ext} takes the following form:

$$Q_{\text{ext}} = \quad m + s\sqrt{m^2 \quad n}, \tag{29}$$

where:

$$m = \frac{(\tau E_s)^2}{2}.s(B_b + B_c + C_2^c), \tag{30}$$

and:

$$n = (\tau E_s)^2.s(C_b + C_1^c \quad C_c), \tag{31}$$

and:

$$s = \text{Sign}(C_c \quad C_b \quad C_1^c). \tag{32}$$

The constants, C_1^c and C_2^c, C_b and B_b and C_c and B_c, are the connector, tank and junction constants, respectively and can be found in [16]. Karney shows that the EED method simplifies the programming and reduces the code size and the simulation time [16].

CROSS CHARACTERISTIC MESH

The cross characteristic mesh is developed in [20], based on the original Brunone model. Here, the same procedure is introduced for the Vitkovsky formulation. By neglecting the convective term with the modified Brunone model, the momentum equation can be rewritten in the following form:

$$L_1 = Q_t + gAH_x + \frac{fQ|Q|}{2DA} + k(Q_t + a\phi_A Q_x) = 0, \tag{33}$$

where $\phi_A = \quad 1$ for $VV_x < 0$ and $\phi_A = +1$ for $VV_x \geq 0$.

Using Equations 33 and 2, Equation 6 will be transformed into:

$$L = Q_t + gAH_x + \frac{fQ|Q|}{2DA} + k(Q_t + a\phi_A Q_x) + \lambda\left(H_t + \frac{a^2}{Ag}Q_x\right) = 0, \tag{34}$$

or, in the rearranged form, as:

$$L{=}\lambda\left[H_t{+}\frac{gA}{\lambda}H_x\right]{+}(1{+}k)\left[Q_t{+}\frac{\lambda a^2{+}gAka\phi_A}{(1{+}k)gA}Q_x\right] + \frac{fQ|Q|}{2DA} = 0. \tag{35}$$

If one writes the following:

$$\frac{dx}{dt} = \frac{gA}{\lambda} = \frac{\lambda a^2 + gAka\phi_A}{(1+k)gA}. \tag{36}$$

Equation 35 is transformed into the ordinary differential equation:

$$\lambda\frac{dH}{dt} + (1+k)\frac{dQ}{dt} + \frac{fQ|Q|}{2DA} = 0. \tag{37}$$

The solution of Equation 36 yields two particular values for λ:

$$\lambda = \quad \frac{gAk}{2a}\phi_A \pm \frac{gA}{2a}(k+2). \tag{38}$$

By using λ as given by Equation 38, Equation 37, for $\phi = \quad 1$ may be rewritten as follows:

$$\frac{dH}{dt} + \frac{a}{gA}(1+k)\frac{dQ}{dt} + a\frac{f}{2gDA^2}Q|Q| = 0, \tag{39}$$

$$\text{on } \frac{dx}{dt} = \quad a, \tag{40}$$

and:

$$\frac{dH}{dt} + \frac{a}{gA}\frac{dQ}{dt} + \frac{a}{1+k}\frac{f}{2gDA^2}Q|Q| = 0, \tag{41}$$

$$\text{on } \frac{dx}{dt} = \frac{a}{1+k}. \tag{42}$$

In the cross characteristic mesh, the intermediate points will be met (see Figures 2 and 3). These points are known as $(i \quad 1, t^*)$ and $(i+1, t^*)$. The unknown discharge and head at these points will be evaluated from the time step, $t \quad \Delta t$ and the desired values at the time t will be estimated from the value at these points. Multiplying Equations 40 and 42 by dt and integrating along their appropriate characteristic lines yields the following:

for the left side of the line, $x = i$;

C^+ :

$$\int_{i\ \ 1,t\ \ \Delta t}^{i\ \ 1,t^*} dH + \frac{a}{gA}\int_{i\ \ 1,t\ \ \Delta t}^{i\ \ 1,t^*} dQ + \frac{f}{2gDA^2}\int_{i\ \ 1,t\ \ \Delta t}^{i\ \ 1,t^*} Q|Q|dx = 0, \tag{43}$$

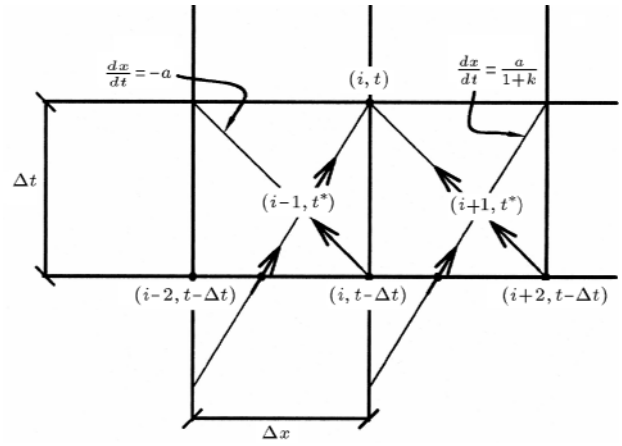

Figure 2. Cross characteristic mesh presented in the previous section for $\phi_A = \quad 1$.

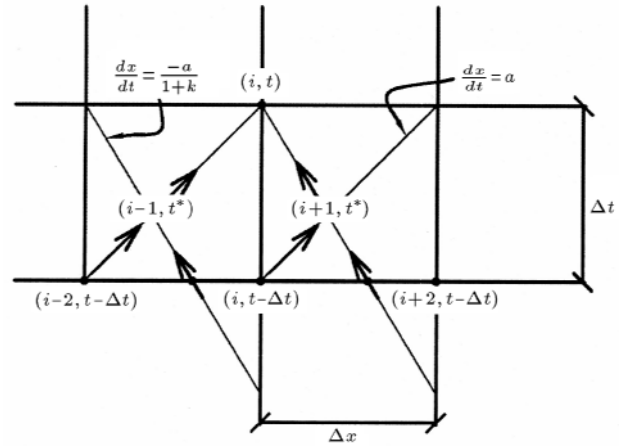

Figure 3. Cross characteristic mesh presented in the previous section for $\phi_A = 1$.

$C \quad :$

$$\int_{i,t \quad \Delta t}^{i \quad 1,t^*} dH \quad \frac{a(1+k)}{gA} \int_{i,t \quad \Delta t}^{i \quad 1,t^*} dQ + \frac{f}{2gDA^2} \int_{i,t \quad \Delta t}^{i \quad 1,t^*} Q|Q|dx = 0, \tag{44}$$

for the right side of the line, $x = i$;

$C^+ :$

$$\int_{i+1,t \quad \Delta t}^{i+1,t^*} dH + \frac{a}{gA} \int_{i+1,t \quad \Delta t}^{i+,t^*} dQ + \frac{f}{2gDA^2} \int_{i+1,t \quad \Delta t}^{i+1,t^*} Q|Q|dx = 0, \tag{45}$$

$C \quad :$

$$\int_{i+2,t \quad \Delta t}^{i+1,t^*} dH \quad \frac{a(1+k)}{gA} \int_{i+2,t \quad \Delta t}^{i+1,t^*} dQ + \frac{f}{2gDA^2} \int_{i+2,t \quad \Delta t}^{i+1,t^*} Q|Q|dx = 0. \tag{46}$$

Using Equation 11 in integrating the last term in Equations 40 to 42, the head-discharge relation will be obtained as follows:

for the left side of the line, $x = i$;

$C^+ :$

$$H_{i \quad 1,t^*} = C_{i \quad 1,t \quad \Delta t} \quad B_{i \quad 1,t \quad \Delta t} Q_{i \quad 1,t^*}, \tag{47}$$

where:

$$C_{i \quad 1,t \quad \Delta t} = H_{i \quad 1,t \quad \Delta t} + Q_{i \quad 1,t \quad \Delta t} \left[B \quad \frac{R}{2} |Q_{i \quad 1,t \quad \Delta t}| (1 \quad \varepsilon) \right], \tag{48}$$

$$B_{i \quad 1,t \quad \Delta t} = B + \frac{R}{2} \varepsilon |Q_{i \quad 1,t \quad \Delta t}|, \tag{49}$$

$C \quad :$

$$H_{i \quad 1,t^*} = C_{i,t \quad \Delta t} + B_{i,t \quad \Delta t} Q_{i \quad 1,t^*}, \tag{50}$$

where:

$$C_{i,t \quad \Delta t} = H_{i,t \quad \Delta t} \quad Q_{i,t \quad \Delta t} \left[B' \quad \frac{R}{2} |Q_{i,t \quad \Delta t}| (1 \quad \varepsilon) \right], \tag{51}$$

$$B_{i,t \quad \Delta t} = B' + \frac{R}{2} \varepsilon |Q_{i,t \quad \Delta t}|, \tag{52}$$

for the right side of the line, $x = i$;

$C^+ :$

$$H_{i+1,t^*} = C_{i+1,t \quad \Delta t} \quad B_{i+1,t \quad \Delta t} Q_{i+1,t^*}, \tag{53}$$

where:

$$C_{i+1,t \quad \Delta t} = H_{i+1,t \quad \Delta t} + Q_{i+1,t \quad \Delta t} \left[B \quad \frac{R}{2} |Q_{i+1,t \quad \Delta t}| (1 \quad \varepsilon) \right], \tag{54}$$

$$B_{i+1,t\ \Delta t} = B + \frac{R}{2}\varepsilon|Q_{i+1,t\ \Delta t}|, \tag{55}$$

C :

$$H_{i+1,t^*} = C_{i+2,t\ \Delta t} + B_{i+2,t\ \Delta t}Q_{i+1,t^*}, \tag{56}$$

where:

$$C_{i+2,t\ \Delta t} = H_{i+2,t\ \Delta t} - Q_{i+2,t\ \Delta t}\left[B' - \frac{R}{2}|Q_{i+2,t\ \Delta t}|(1-\varepsilon)\right], \tag{57}$$

$$B_{i+2,t\ \Delta t} = B' + \frac{R}{2}\varepsilon|Q_{i+2,t\ \Delta t}|. \tag{58}$$

With $B = \frac{a}{gA}$, $B' = (1+k)B$ and $R = \frac{f}{2gDA^2}$.

Using the same procedure, the relation between head and discharge at the point (i,t) can be found as follows:

for the left side of the line, $x = i$;

C^+ :

$$H_{i,t} = C_{i\ 1,t^*} - B_{i\ 1,t^*}Q_{i,t}, \tag{59}$$

for the right side of the line, $x = i$;

C^- :

$$H_{i,t} = C_{i+1,t^*} + B_{i+1,t^*}Q_{i,t}. \tag{60}$$

It can be seen that the constants $C_{i\ 1,t^*}$ and $B_{i\ 1,t^*}$ are functions of $Q_{i\ 1,t^*}$, which can be evaluated by simultaneously solving Equations 47 and 50, resulting in:

$$Q_{i\ 1,t^*} = \frac{C_{i\ 1,t\ \Delta t} - C_{i,t\ \Delta t}}{B_{i\ 1,t\ \Delta t} + B_{i,t\ \Delta t}}. \tag{61}$$

The same procedure can be used to find Q_{i+1,t^*}, as follows:

$$Q_{i+1,t^*} = \frac{C_{i+1,t\ \Delta t} - C_{i+2,t\ \Delta t}}{B_{i+2,t\ \Delta t} + B_{i+1,t\ \Delta t}}. \tag{62}$$

TEST CASE AND RESULTS

The effect of the unsteady friction term is tested, based on the example in [16]. The layout of the system, consisting of seven pipes and seven nodes, is presented in Figure 4. The data specifications of the system are given in Tables 1 to 3. Table 1 contains the nodal steady-state data while Tables 2 and 3 refer to the pipe physical data, initial flows and the data specification for external dissipative devices, respectively. The transient behavior of the system, caused by the following operation of the control valve located at node 7, is analyzed for 60 s [16]:

Case 1. The control valve opening, "τ", decreases linearly from $\tau = 0.6$ to $\tau = 0.2$ in 10 s (Figure 5).

Case 2. The control valve opening, "τ", decreases linearly from $\tau = 0.6$ to $\tau = 0.2$ in 10 s, maintained for 15 s and, then, increases linearly to its initial value of $\tau = 0.6$ in 5 s (Figure 6).

The time step selected for the computer simulations was approximately 0.1 s. The pipe system was discretized into 90 pipe reaches, according to [16]. In order to validate the present code, results are compared with the results of [16] and, then, the effects of the unsteady friction term were investigated. Figures 7 and 8 show the hydraulic grade-line elevation and external flow at node 7 for Cases 1 and 2, respectively. There is close correspondence between the results of the present code and [16].

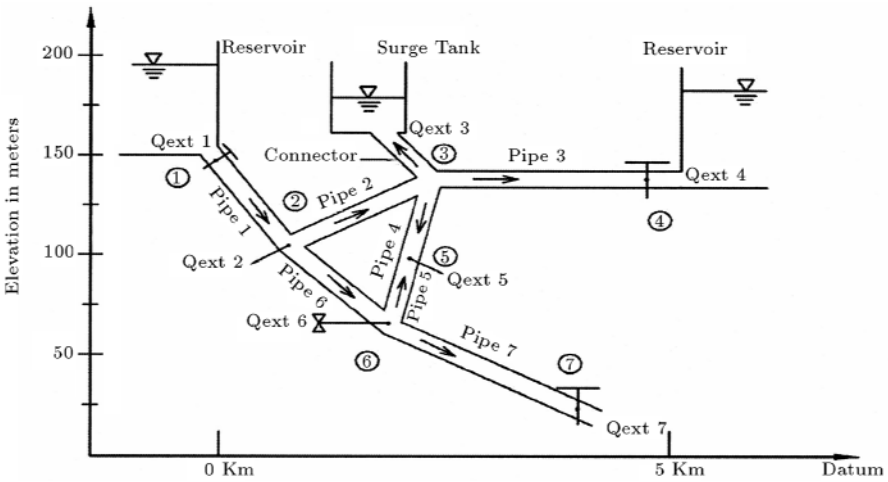

Figure 4. Definition diagram for simple network.

Table 1. Nodal steady-state data.

Node Number	Elevation (m)	Hydraulic Grade-Line Elevation (m)	Q_{ext_i} (m/s^2)	Device Description
1	150	200.0	-6.211	Constant head reservoir
2	100	195.0	+2.000	Constant demand
3	150	188.8	+0.000	Surge tank
4	150	175.0	+1.183	Constant head reservoir
5	100	183.4	+1.000	Constant demand
6	50	187.9	+0.000	Constant relief valve
7	25	151.9	+2.028	Control valve

Table 2. Pipe physical data and initial flow.

Pipe Number	From Node	To Node	Initial Flow (m/s^2)	Length (m)	Diameter (m)	Wave Speed (m/s)	Darcy Friction
1	1	2	6.212	1001.2	1.500	996.3	0.012
2	2	3	1.708	2000.0	1.000	995.3	0.013
3	3	4	1.183	2000.0	0.750	995.0	0.014
4	3	5	0.524	502.5	0.500	1000.0	0.015
5	6	5	0.476	502.5	0.500	1000.0	0.015
6	2	6	2.503	1001.2	1.000	996.3	0.014
7	6	7	2.028	2000.2	0.750	995.3	0.013

Table 3. Data specification for external dissipative device.

External Flow Device	Valve/Orifice		Tank/Reservoir				Connector		
	E $\left(\frac{m^{\frac{5}{2}}}{s}\right)$	E $\left(\frac{m^{\frac{5}{2}}}{s}\right)$	Z_{bot} (m)	Z_{top} (m)	A_r (m^2)	f_r	L_c (m)	D_c (m)	f_c
Q_{ext_1}	5.0	5.0	150	201.5	∞	0	0	> 0	0
Q_{ext_3}	3.0	3.0	180	195.0	5.0	0.020	30	0.500	0.020
Q_{ext_4}	1.0	1.0	150	173.6	∞	0	0	> 0	0
Q_{ext_6}	0.0	0.0	50	50.0	∞	0	0	> 0	0
Q_{ext_7}	0.0	0.0	25	25.0	∞	0	0	> 0	0

Figures 9 and 10 show the hydraulic grade-line elevation and external flow at nodes 7 and 6 for Cases 1 and 2, respectively. Figure 11 shows that, during the first 20 s, the system has nearly the same response. Also, it is shown that the peak head is identical in both cases. After this time, each curve has its own behavior and they are clearly different. The reopening of the control valve at node 7 causes an increasing demand at node 7 and will result in a severe pressure drop. In this case, a reversal in the flow direction of the surge tank would occur. The effect of the valve can be regarded as the perturbations to the system. If the perturbations to the system are of the second case, damage to the system will be far more. Figures 9 and 10 show the differences when k increases. In both cases, k is changed from 0 to 0.2 and 0.4, where $k = 0$ refers to the steady-state friction model. One significance of coefficient k is in filtering the curves, so that k can act as a low pass filter. These figures show that damping effects will increase if k increases. Another, and the most important, effect of the unsteady friction term can be seen in the damping of the pressure waves traveling along the system when the valve is set to be closed. From the results of the different values for k, it can be slightly indicated that the nature of the response depends more on how the pressure peak decays from one cycle to the next, not simply on the peak pressures for the first cycle. An obvious shift of the head peaks can be seen in Figures 9

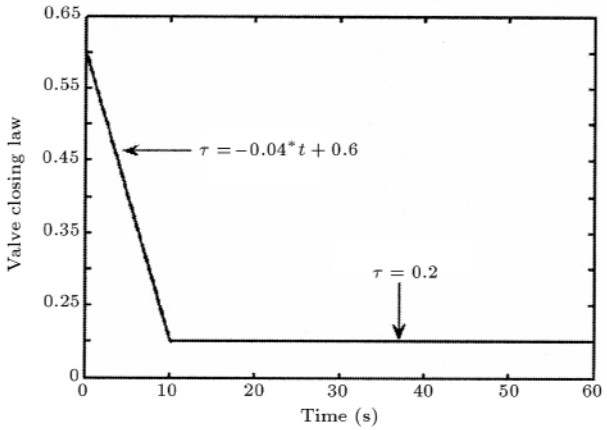

Figure 5. Valve closing law for Case 1.

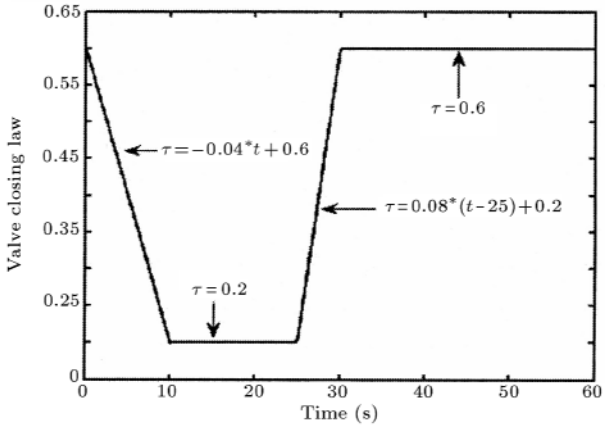

Figure 6. Valve closing law for Case 2.

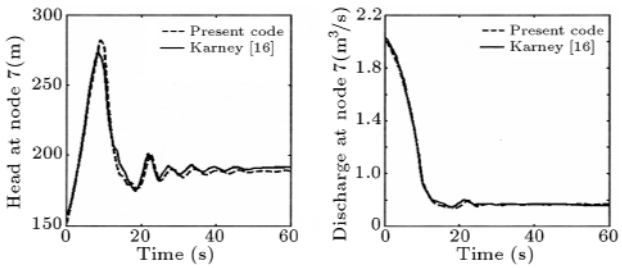

Figure 7. Comparison between the hydraulic grade-line elevation and the external flow at node 7 with [16] in Case 1.

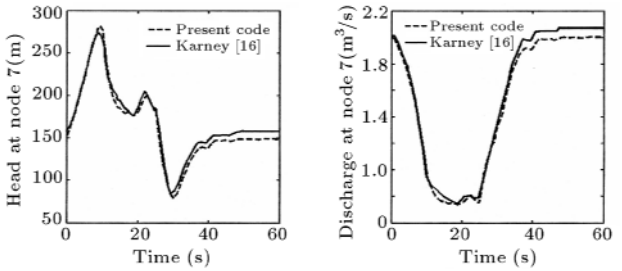

Figure 8. Comparison between the hydraulic grade-line elevation and the external flow at node 7 with [16] in Case 2.

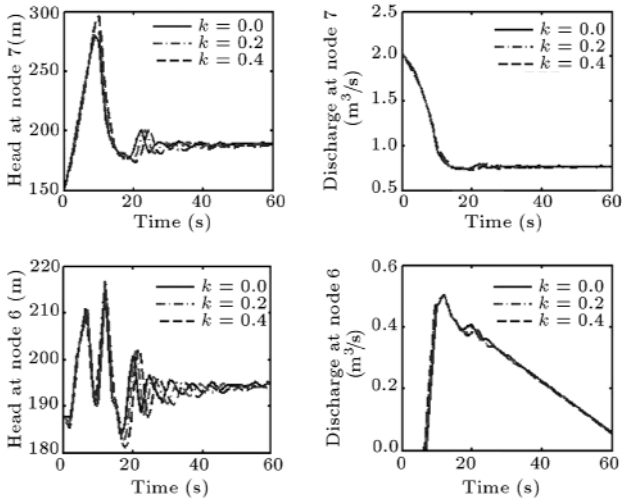

Figure 9. Hydraulic grade-line elevation and external flows at selected locations: Case 1.

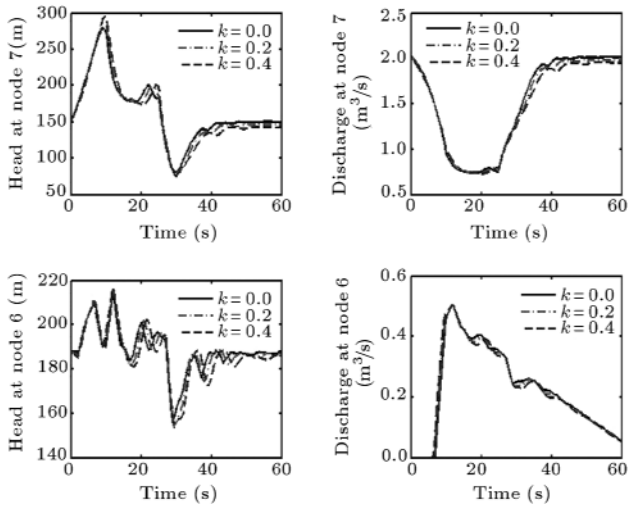

Figure 10. Hydraulic grade-line elevation and external flows at selected locations: Case 2.

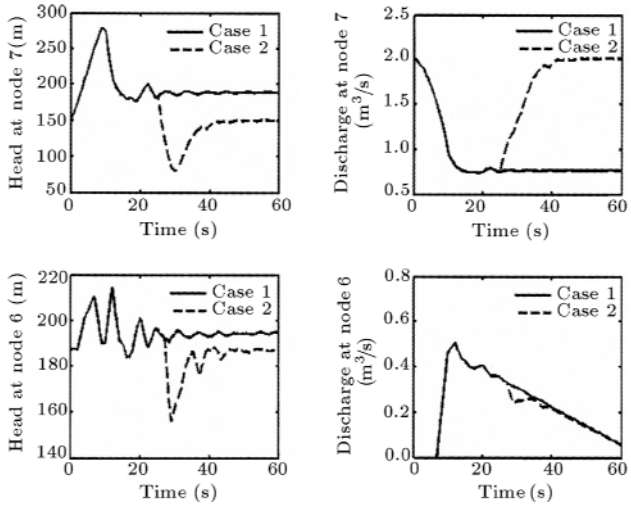

Figure 11. Comparison between two cases for $k = 0$.

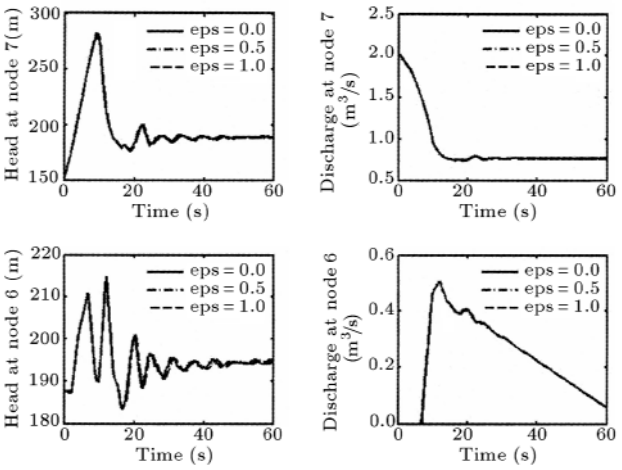

Figure 12. Effect of the weighting term in the integration of the friction-loss: Case 1.

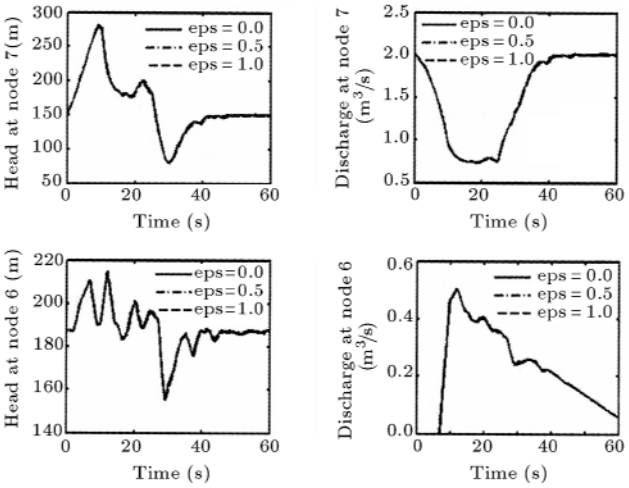

Figure 13. Effect of the weighting term in the integration of the friction-loss : Case 2.

and 10. In Figures 12 and 13, the dependence of the results on the linearization constant is shown. From these figures it is clear that the tendency of the results for different values of ε is the same. So, using the previous time step values in the integrating of the friction term will predict events reasonably enough.

CONCLUSION

The results from the quasi-steady friction model ($k = 0$ in the Brunone model) and the Brunone model have been compared with each other for the closing of a control valve at the downstream of a simple network. The results showed the importance of considering the unsteady friction term in the transient-state condition during the design process. The more coefficient k increases in the Brunone model, the more it decays the traveling pressure wave. Thus, knowing the best value for k in each case depends on the empirical results. On the other hand, if the maximum head rise is practically considered, there is no need to pay for the unsteady friction term, which considers the decay phase and not the maximum phase. Moreover, for reducing the number of boundary conditions, the EED method has been used. This method can demonstrate many complex devices in a general element (EED). Thus, by using this method, the process of programming will become simplified, the code size will be reduced and the simulation time will decrease. The effect of the linearization constant has been incorporated in the simple form of the friction term integration. It is seen that the results did not have a clear dependence on different linearization constants in the integrating of the friction term, from the explicit to implicit method for the text network.

NOMENCLATURE

A	cross-sectional area of the pipe
a	wave speed
B_{c+}	constant
B_c	constant
B	constant
B'	constant
C_1^c, C_2^c	connector constants
C_b, B_b	tank constants
C_c, B_c	junction constants
C	negative characteristic line
C^+	positive characteristic line
C_{c+}	constant
C_c	constant
C^*	Vardy and Brown's shear decay coefficient
D	pipe diameter
E_s	valve/orifice parameters
f	Darcy-Weisbach friction factor
f_q	quasi-steady part of the friction factor
f_u	unsteady part of the friction factor
g	gravitational acceleration
H	piezometric head
H_p^c	head at the node side of the connector
h_f	energy loss per unit weight
i	ith cross-section
k	constant
L	pipe length
Q	discharge
Q_{ext}	external flow
R	constant
r	radial direction

t	time
Δt	time step
u'	fluctuation of the u velocity in the axial direction
V	fluid velocity
v'	fluctuation of the v velocity in the radial direction
W	weight for the past acceleration
x	distance along pipe

Greek Symbols

λ	unknown multiplier
μ	fluid viscosity
ρ	fluid density
ε	linearization constant
τ	dimensionless time
υ	kinematic viscosity
ϕ_L	headloss due to fluid friction per unit length

REFERENCES

1. Holmboe, E.L. and Rouleau, W.T. "The effect of viscous shear on transients in liquid lines", *Journal of Basic Engineering*, **89**, pp 174-180 (1967).
2. Zielke, W. "Frequency-dependent friction in transient pipe flow", *Journal of Basic Engineering*, **90**(1), pp 109-115 (1968).
3. Vardy, A.E., Brown, J.M.B. and Hwang, K.L. "A weighting function model of transient turbulent pipe friction", *Journal of Hydraulic Research*, **31**(4), pp 533-548 (1993).
4. Ghidaoui, M.S. and Mansour, S. "Efficient treatment of the Vardy-Brown unsteady shear in pipe transients", *Journal of Hydraulic Engineering, ASCE*, **128**(1), pp 102-112 (2002).
5. Brunone, B., Karney, W., Mecarelli, M. and Ferrante, M. "Velocity profiles and unsteady pipe friction in transient flow", *Journal of Water Resources Planning and Management*, **126**(4), pp 236-244 (2000).
6. Silva-Araya, W.F. and Chaudhry, M.H. "Computation of energy dissipation in transient flow", *Journal of Hydraulic Engineering, ASCE*, **123**(2), pp 108-115 (1997).
7. Vardy, A.E. and Hwang, K.L. "Characteristic model of transient friction in pipes", *Journal of Hydraulic Research*, **29**(5), pp 669-684 (1991).
8. Brunone, B., Golia, U.M. and Greco, M. "Effects of two-dimensionality on pipe transients modeling", *Journal of Hydraulic Engineering*, **121**(12), pp 906-912 (1995).
9. Pezzinga, G. "Quasi-2D model for unsteady flow in pipe networks", *Journal of Hydraulic Egineering, ASCE*, **125**(7), pp 676-685 (1999).
10. Bergant, A., Simpsom, A.R. and Vitkovsky, J.P. "Developments in unsteady pipe flow friction modeling", *Journal of Hydraulic Research*, **39**(3), pp 249-257 (2001).
11. Trikha, A.K. "An efficient method for simulating frequency-dependent friction in transient liquid flow", *Journal of Fluids Engineering, ASCE*, pp 97-105 (1975).
12. Suzuki, K., Taketomi, T. and Sato, S. "Improved Zielke's method of simulating frequency-dependent friction in laminar pipe flow", *Journal of Fluid Engineering, ASCE*, **113**(4), pp 569-573 (1991).
13. Schohl, G.A. "Improved approximate method for simulating frequency-development friction in transient laminar flow", *Journal of Fluids Engineering, ASCE*, **115**, pp 420-424 (1993).
14. Vardy, A.E. and Brown, J.M.B. "Transient, turbulent, smooth pipe friction", *Journal of Hydraulic Research*, **33**(4), pp 435-455 (1995).
15. Bergant, A., Vitkovsky, J.P., Simpson, A.R. and Lambert, M. "Behavior of unsteady pipe flow friction models in the case of valve-opening", *Proceeding of the 21st IAHR Symposium on Hydraulic Machinery and Systems*, Lausanne (Sept. 2002).
16. Karney, B.W. and McInnis, D. "Efficient calculation of transient flow in simple pipe networks", *Journal of Hydraulic Engineering, ASCE*, **118**(7), pp 1014-1030 (1992).
17. Wylie, E.B. and Streeter, V.L., *Fluid Transients*, FEB Press, Ann Arbor, Michigan, USA (1982).
18. Chaudhry, M.H., *Applied Hydraulic Transients*, Van Nostrand Reihold, New York, NY, USA (1979).
19. Larock, B.E., Jeppson, R.W. and Watters, G.Z., *Hydraulics of Pipe Line Systems*, CRC Press, N.W., Boca Raton, Florida, USA (2000).
20. Poll, H. "The importance of the unsteady friction term of the momentum equation for hydraulic transients", *Proceeding of the 21st IAHR Symposium on Hydraulic Machinery and Systems*, Lausanne (Sept. 2002).